Secondary Control Scheme for Voltage Unbalance Compensation in an Islanded Droop-Controlled Microgrid

Savaghebi, Mehdi; Jalilian, Alireza ; Vasquez, Juan Carlos; Guerrero, Josep M.

Published in:
IEEE Transactions on Smart Grid

DOI (link to publication from Publisher):
10.1109/TSG.2011.2181432

Publication date:
2012

Document Version
Early version, also known as pre-print

Secondary Control Scheme for Voltage Unbalance Compensation in an Islanded Droop-Controlled Microgrid

Mehdi Savaghebi, *Student Member*, *IEEE*, Alireza Jalilian, Juan C. Vasquez, and Josep M. Guerrero, *Senior Member, IEEE*

***Abstract*— The concept of microgrid hierarchical control is presented recently. In this paper, a hierarchical scheme is proposed which includes primary and secondary control levels. The primary level comprises distributed generators (DGs) local controllers. The local controllers mainly consist of power, voltage and current controllers, and virtual impedance control loop. The central secondary controller is designed to manage the compensation of voltage unbalance at the point of common coupling (PCC) in an islanded microgrid. Unbalance compensation is achieved by sending proper control signals to the DGs local controllers. The design procedure of the control system is discussed in detail and the simulation results are presented. The results show the effectiveness of the proposed control structure in compensating the voltage unbalance.**

***Index Terms*—Distributed generator (DG), hierarchical control, microgrid, secondary control, voltage unbalance compensation.**

I. Introduction

THE term "smart grid" is usually applied to describe a power system which utilizes advanced sensing and monitoring system as well as information and communication technology (ICT) in order to improve the performance of the grid and provide a wide range of additional services for the consumers [1], [2].

The smart grid can be seen as a collection of technologies, concepts and approaches for gradual conversion from the traditional hierarchies of generation, transmission and distribution to an intelligent, distributed, end-to-end structure. Smart grid is a grid that accommodates several power generation options such as central, distributed and mobile. In a smart grid the consumers are able to interact with an energy management system in order to adjust the energy consumption and reduce the energy cost [3].

Some of the attributes which are commonly cited for smart grids are as follow [1]-[8]:

- Self-healing from power disturbances
- Economical based on efficient energy management and optimized asset utilization
- Automated based on the high penetration of ICT and advanced metering infrastructure
- Enabling new products, services, and markets
- Providing high power quality and reliability
- Integrating distributed power generation and storage
- Utilizing renewable energy resources to advance energy sustainability and address environmental concerns

On the other hand, microgrids are low-voltage distribution networks comprising various distributed resources (DRs) and different types of loads and are able to operate either interconnected to the main distribution grid or isolated from it (grid-connected and islanded operation modes, respectively). DRs may include both DGs and distributed storage units [9]-[11].

Microgrids are deemed as one of the main building blocks of the smart grids; since, are able to facilitate implementation of many smart grid functions [3]-[5]. It is expected that in a near future, smart grid emerges as a well-planned plug-and-play integration of microgrids which interact through dedicated highways for exchanging commands, data, and power [3]. Considering the aforementioned smart grid attributes, it should be noted that the microgrid DGs prime-movers are mainly no-emission renewable energy resources. Furthermore, the power electronic interface converter (e.g. an inverter in the case of dc-to-ac conversion) which is often used to connect the DGs to the electrical system can provide several control functionalities.

In fact, the main role of the DG inverter is to adjust output voltage phase angle and amplitude in order to control the active and reactive power injection. However, compensation of power quality problems can also be achieved through proper control strategies.

Amongst various power quality phenomena, voltage unbalances are very common. Voltage unbalance can result in adverse effects on the equipment and power system. Under unbalanced conditions, the power system will incur more losses and be less stable. Also, voltage unbalance has some negative impacts on equipment such as induction motors, power electronic converters and adjustable speed drives (ASDs). Thus, the International Electrotechnical Commission (IEC) recommends the limit of 2% for voltage unbalance in electrical systems [12]. A major cause of voltage unbalance is the connection of unbalanced loads (mainly, single-phase

M. Savaghebi and A. Jalilian are with the Electrical Engineering Department and Center of Excellence for Power System Automation and Operation, Iran University of Science and Technology, Tehran 16846-13114, Iran (e-mails: savaghebi@iust.ac.ir, jalilian@iust.ac.ir).

J. C. Vasquez is with the Institute of Energy Technology, Aalborg University, Aalborg East DK-9220, Denmark (e-mail: juq@et.aau.dk).

J. M. Guerrero is with the Institute of Energy Technology, Aalborg University, Aalborg East DK-9220, Denmark and the Department of Automatic Control and Industrial Informatics, Technical University of Catalonia (UPC), 08036 Barcelona, Spain (e-mail: joz@et.aau.dk).

loads connection between two phases or between one phase and the neutral).

Compensation of voltage unbalance is usually done using series active power filter through injection of negative sequence voltage in series with the power distribution line [13]-[15]. However, there are a few works [16]-[19] based on using shunt active power filter for voltage unbalance compensation. In these works, voltage unbalance caused by unbalanced load is compensated through balancing the line currents.

In [20]-[23], some approaches are presented to use the DG for voltage unbalance compensation. A method for voltage unbalance compensation through injection of negative sequence current by the DG has been proposed in [20]. By applying this method, the line currents become balanced in spite of unbalanced loads presence. However, under severely unbalanced conditions, a large amount of the interface converter capacity is used for compensation and it may interfere with the active and reactive power supply by the DG.

The approach presented in [21] is based on controlling the DG as a negative sequence conductance to compensate the voltage unbalance at the microgrid DGs terminal. In this approach which is implemented in the synchronous (dq) reference frame, compensation is done by generating a reference for negative sequence conductance based on the negative sequence reactive power. Then, this conductance is applied to produce the compensation reference current.

In [21] the compensation reference is injected to the output of the voltage controller. As explained in [22], this place of compensation reference injection is not proper, since the voltage controller considers this reference as a disturbance. Thus, it is proposed in [22] to inject the compensation reference before the voltage controller. It is noteworthy that the control system of [22] is designed in stationary ($\alpha\beta$) reference frame. A similar control structure is applied in [23] for a grid-connected DG. In [23] a proportional-integral (PI) controller is used to follow the reference of the voltage unbalance factor.

The methods proposed in [21]-[23] are designed for compensation of voltage unbalance at the DG terminal, while usually the power quality at the point of common coupling (PCC) is the main concern due to sensitive loads which may be connected. Thus, in this paper the concept of microgrid secondary control [24]-[27] is applied to compensate the voltage unbalance at PCC in an islanded microgrid. Furthermore, the design and stability analysis of the control system is addressed. In the proposed control structure, a PI controller is used to generate the reference of unbalance compensation for the DGs of the microgrid. This reference is transmitted through low bandwidth communication links to the DG local controllers which constitute the primary control level.

The rest of the paper is organized as follows. The structure of the microgrid hierarchical control and the details of secondary level are discussed in Section II. Section III is dedicated to the proposed DG local control strategy. The design approach of the control system is presented in Section IV. Section V includes simulation results. Finally, the paper is concluded in Section VI.

II. Microgrid Hierarchical Control Scheme

The control of the microgrid may be done based on the autonomous operation of DGs local controllers (decentralized control, e.g. [21], [22], [28]-[33]) or be managed by a central controller (centralized control, e.g. [11], [24]-[27], [34]-[36]). The centralized control can be achieved according to a hierarchical control structure which consists of different control levels.

A hierarchical control structure consisting of three control levels is proposed in [11]. The control levels are local microsource and load controllers (MC/LC), microgrid central controller (MGCC) and distribution management system (DMS). When the microgrid operates in grid-connected mode, MCs follow the commands from the MGCC. In islanded mode, MCs perform local optimization of the DG active and reactive power production, and fast load tracking. LCs are installed at the controllable loads location and act based on the commands of MGCC. Economic optimization of microgrid operation considering market conditions and fuel consumption is also performed by the MGCC.

Similar hierarchical structures which are mainly focused on the economic optimization of microgrid operation based on the multi-agent systems are proposed in [34]-[36].

Economic optimization of the microgrid operation falls out of the present paper scope.

It is noteworthy that when the microgrid operates in islanded mode, the voltage and frequency should be supported by the DGs, while in grid-connected mode the support is provided by the main grid. Frequency control is a challenging problem in islanded operation, since the microgrids mainly comprise converter-connected inertia-less DGs [37]. However, some virtual inertia can be provided by the power droop controllers [24].

The hierarchical control scheme of [24] is organized in three-levels: primary, secondary and tertiary. The primary control deals with the local control of the DG units. The secondary level is designed to restore the DGs output voltage frequency and amplitude deviations which are produced by the power droop controllers and output impedances.

A similar approach for frequency restoration is adapted in [33], but, instead of a central secondary control, a PI controller is added locally in the droop controller of each DG. This way, the communication link is not necessary; but, small inevitable differences among local estimations of frequency are integrated over time and lead to circulating power among DGs [38]. To cope with this problem, it is proposed in [38] to use a dead-band block before the PI controller. The width of the dead-zone must be greater than the maximum frequency estimation error. However, this problem is solved at the expense of steady state error in frequency control and active power sharing as can be seen in the results presented in [38].

Both local and central frequency restoration approaches as well as the effect of dynamic response of the DGs on the frequency restoration are discussed in [25].

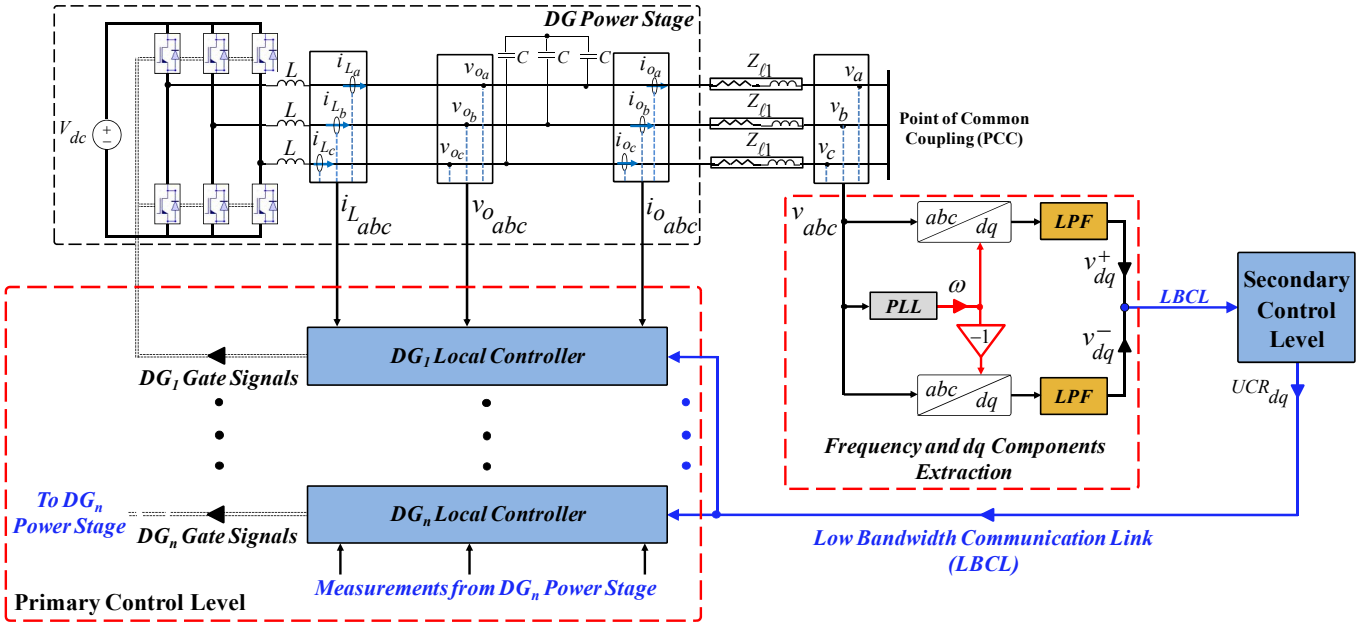

Fig. 1. Power stage and hierarchical control scheme.

The tertiary control level regulates the power exchange between the grid and the microgrid [24],[39],[40]. Since, in the present paper, the microgrid operates in islanded mode, this control level is not considered.

The main focus of the present paper is on the voltage quality at PCC. The proposed hierarchical control structure and the DG power stage are shown in Fig. 1. As seen, the power stage of each DG consists of a DC prime mover, an interface inverter and an LC filter. $Z_{\ell 1}$ models the distribution line between DG_1 and PCC. For simplicity, only the power stage and tie line of DG_1 are depicted. The other microgrid DGs have the same power stage, but, can be connected to PCC through different line impedances.

As seen in Fig. 1, the local controllers generate the gate signals for DGs interface inverters. The local controller of each DG consists of voltage and current controllers, virtual impedance loop and active/reactive power droop controllers. More details are provided in the next Section.

The secondary controller manages the unbalance compensation of microgrid PCC voltage by sending proper control signals to the DGs local controllers. Unbalance compensation as a new feature of the secondary controller is the main contribution of the present paper.

The secondary controller can be far from DGs and PCC. Thus, as shown in Fig. 1, a low bandwidth communication link (*LBCL*) is considered to send the PCC voltage information to this controller. Also, the control signal for voltage unbalance compensation (UCR_{dq}: *Unbalance Compensation Reference*) is transmitted by means of *LBCL* to the primary level.

In order to ensure that low bandwidth is sufficient, the transmitted data should be approximately dc signals. Thus, the data are transmitted in *dq* reference frame.

As shown in Fig. 1, microgrid angular frequency (ω) is estimated by a phase-locked loop (*PLL*) block. Then, in order to extract PCC voltage positive and negative sequences, v_{abc} is transformed to *dq* reference frames rotating at the speeds ω and $-\omega$, respectively. The transformation matrix can be found in [41].

Afterwards, two 2nd order low-pass filters (*LPF*) are used to extract positive and negative sequences (v_{dq}^{+} and v_{dq}^{-}, respectively). 2nd order *LPF*s are applied, since, the 1st order ones cannot provide acceptable filtering. The transfer function of *LPF*s is as follows:

$$LPF = \frac{\omega_{cut}^2}{s^2 + 2\zeta\omega_{cut}s + \omega_{cut}^2} \quad (1)$$

where ω_{cut} and ζ are the filter cut-off frequency and damping ratio, respectively ($\omega_{cut}=4\pi$ (*rad/sec*) and $\zeta=0.707$).

Finally, v_{dq}^{+} and v_{dq}^{-} signals are transmitted toward the secondary controller. The block diagram of the secondary controller is shown in Fig. 2. As can be seen, v_{dq}^{+} and v_{dq}^{-} are used to calculate "*Voltage Unbalance Factor (VUF)*". Then, the calculated value is compared with the reference *VUF* (*VUF**) and the error is fed to a PI controller. Afterwards, the output of PI controller is multiplied by v_{dq}^{-} to generate UCR_{dq} which is transmitted to the primary level.

In fact, data communication is not a critical issue in the proposed hierarchical structure; since, the primary control is performed autonomously according to the local measurements; furthermore, transmission of PCC voltage information and global unbalance compensation reference, respectively to the secondary and primary levels, does not require a high bandwidth due to the use of *dq* coordinates. This way, the control system reliability is improved, since compensation is not dependent on the presence of high communication bandwidth.

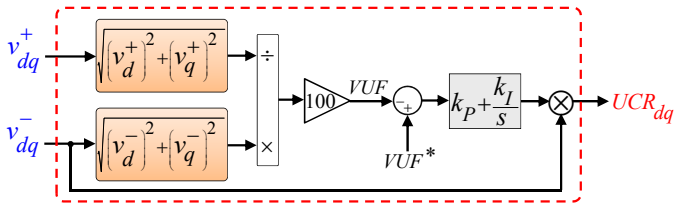

Fig. 2. Block diagram of secondary control level.

As shown in Fig. 3, at first, UCR_{dq} is transformed to $\alpha\beta$ frame and then added as a reference for voltage controller. It is noteworthy that this transformation is performed over negative sequence values; thus, $-\phi^*$ is used as the rotation angle. ϕ^* is the DG voltage reference phase angle which is generated by active power droop controller as explained in Subsection III-A. The transformation matrix can be found in [42].

III. DG Inverter Local Control System

The DG local control system shown in Fig. 3 is designed in $\alpha\beta$ reference frame. So, Clarke transformation is used to transform the variables between *abc* and $\alpha\beta$ frames. The transformation matrices are presented in [22].

As shown in Fig. 3, the voltage controller follows the references generated by power controllers and secondary level to generate the reference for the current controller.

The output of the current controller is transformed back to *abc* frame to provide three-phase voltage reference for the pulse width modulator (*PWM*). Finally, the *PWM* block controls the switching of the inverter based on this reference. More details are provided in the following Subsections.

A. Active and Reactive Power Control

Considering a DG connected to the grid through the impedance $Z\angle\theta$, the active and reactive powers injected to the grid by the DG can be expressed as follows [28]:

$$P=\left(\frac{EV}{Z}\cos\phi-\frac{V^2}{Z}\right)\cos\theta+\frac{EV}{Z}\sin\phi\sin\theta \tag{2}$$

$$Q=\left(\frac{EV}{Z}\cos\phi-\frac{V^2}{Z}\right)\sin\theta-\frac{EV}{Z}\sin\phi\cos\theta \tag{3}$$

where E is the magnitude of the inverter output voltage, V is the grid voltage magnitude, ϕ is the load angle (the angle between E and V), and Z and θ are the magnitude and the phase angle of the impedance, respectively. Considering phase angle of the grid voltage to be zero, ϕ will be equal to phase angle of the inverter voltage.

Assuming mainly inductive electrical systems ($Z\approx X$ and $\theta\approx 90$), the active and reactive powers can be expressed as the following equations:

$$P\approx\frac{EV}{X}\sin\phi \tag{4}$$

$$Q\approx\frac{EV\cos\phi-V^2}{X} \tag{5}$$

In practical applications, ϕ is normally small; thus, a P/Q decoupling approximation ($\cos\phi\approx 1$ and $\sin\phi\approx\phi$) can be considered as follows [28], [29]:

$$P\approx\frac{EV}{X}\phi \tag{6}$$

$$Q\approx\frac{V}{X}(E-V) \tag{7}$$

Thus, active and reactive powers can be controlled by the DG output voltage phase angle and amplitude, respectively. According to this, the following droop characteristics are applied for the positive sequence active and reactive power sharing among DGs in an islanded microgrid:

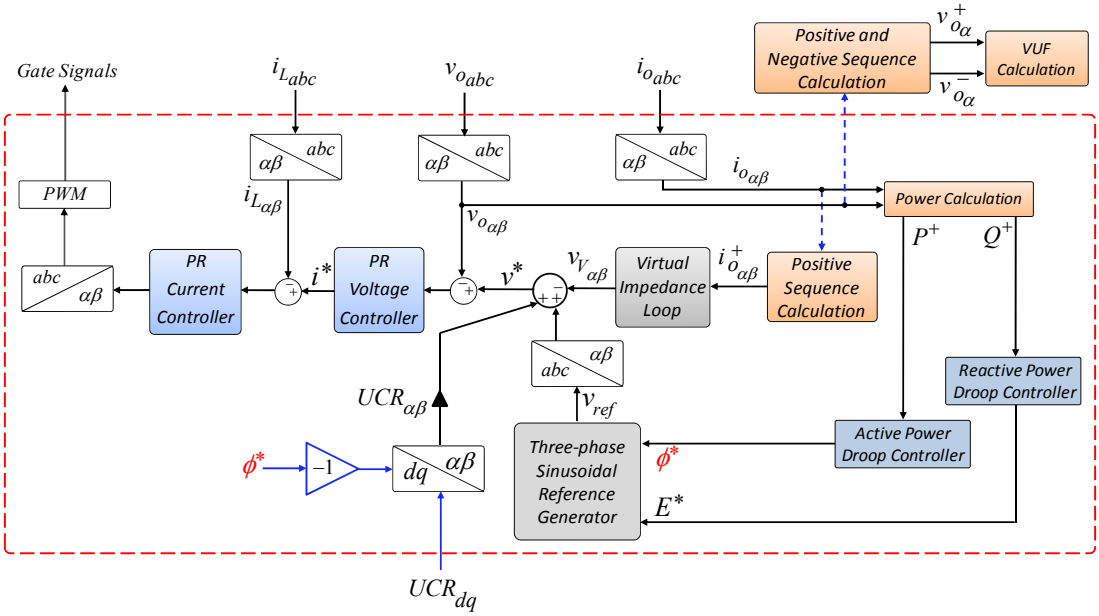

Fig. 3. Schematic diagram of DG local controller.

$$\phi^* = \frac{\omega^*}{s} = \frac{1}{s}\left[\omega_0 - (m_P + m_D s)P^+\right] \quad (8)$$

$$E^* = E_0 - n_P Q^+ \quad (9)$$

where

- s: Laplace variable
- E_0 : rated voltage amplitude
- ω_0 : rated angular frequency
- P^+ : positive sequence active power
- Q^+ : positive sequence reactive power
- m_P : active power proportional coefficient
- m_D : active power derivative coefficient
- n_P : reactive power proportional coefficient
- E^* : voltage amplitude reference
- ϕ^* : voltage phase angle reference
- ω^* : angular frequency reference

The derivative coefficient in equation (8), m_D, helps to improve the dynamic behavior of the power control [28]. It is noteworthy that according to the equations (8) and (9), no integral term is considered for voltage frequency and amplitude control. If the microgrid operates in islanded mode (the case considered in this paper) the use of pure integrators is not allowed; since, the total load will not coincide with the total injected power, and it leads to instability [24], [30].

As can be seen in Fig. 3, E^* and ϕ^* are used to generate the three phase reference voltage (v_{ref}). This voltage is positive-sequence component; thus positive sequence powers (P^+ and Q^+) are used in equations (8) and (9).

According to Fig. 3, at first DG three-phase output voltage and current ($v_{o_{abc}}$ and $i_{o_{abc}}$, respectively) are measured and transformed to $\alpha\beta$ frame ($v_{o_{\alpha\beta}}$ and $i_{o_{\alpha\beta}}$, respectively). Then, positive and negative sequences of output voltage and positive sequence of output current are extracted [43], [44]. Positive sequence current is fed to the virtual impedance block. Also, positive and negative sequences of output voltage are applied for *VUF* calculation. The calculated *VUF* is not used in the control system and just will be shown in Section V to demonstrate the effect of control system action on the DGs *VUF*. The details of this calculation are shown in Fig. 4. As can be seen, α-components of DG output voltage positive and negative sequences are fed to *VUF* calculation block. Then, the average values of rectified waveforms ($\bar{v}_{o_\alpha}^+$ and $\bar{v}_{o_\alpha}^-$) are calculated by applying two absolute functions (*abs*) and low-pass filters (*LPF*). *LPF* structure and parameters are exactly same as equation (1). Finally, calculation of *VUF* is done by division of $\bar{v}_{o_\alpha}^-$ by $\bar{v}_{o_\alpha}^+$. It is noteworthy that if the β-components are used for *VUF* calculation, the result will be the same, because, the positive and negative sequences are balanced. In the other words, α- and β-components of positive (or negative) sequence have equal amplitudes.

B. Power Calculation

Based on the instantaneous reactive power theory [45], the instantaneous values of active and reactive powers should be calculated using equations (10) and (11), respectively:

$$p = v_{o_\alpha} i_{o_\alpha} + v_{o_\beta} i_{o_\beta} \quad (10)$$

$$q = v_{o_\beta} i_{o_\alpha} - v_{o_\alpha} i_{o_\beta} \quad (11)$$

Each of the instantaneous powers consists of dc and ac (oscillatory) components. The dc components (average values of p and q) are positive sequence active and reactive powers (P^+ and Q^+, respectively) [46]. The oscillatory parts are generated by the unbalance and/or harmonic contents of the voltage and current.

The dc components are extracted using two 1st order low pass filters. The cut-off frequency of these filters is set to 4π (*rad/sec*).

C. Virtual Impedance Loop

Addition of the virtual resistance makes the oscillations of the system more damped [28]. In contrast with physical resistance, the virtual resistance has no power losses, and it is possible to implement it without decreasing the efficiency.

Also, the virtual inductance is considered to ensure the decoupling of P and Q. Thus, virtual impedance makes the droop controllers more stable [31].

The virtual impedance can be achieved as shown in Fig. 5, where R_v and L_v are the virtual resistance and inductance, respectively [32]. According to this Fig., the following equations are extracted:

$$v_{V_\alpha} = R_v \cdot i_{o_\alpha}^+ - L_v \cdot \omega \cdot i_{o_\beta}^+ \quad (12)$$

$$v_{V_\beta} = R_v \cdot i_{o_\beta}^+ + L_v \cdot \omega \cdot i_{o_\alpha}^+ \quad (13)$$

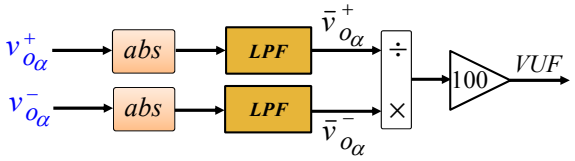

Fig. 4. Block diagram of *VUF* calculation in $\alpha\beta$ frame.

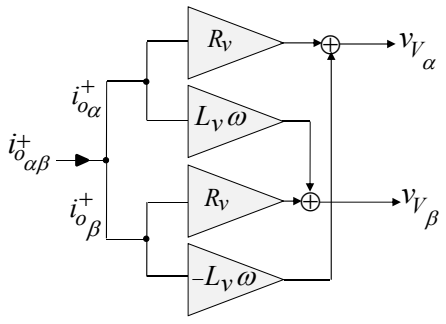

Fig. 5. Virtual impedance block diagram.

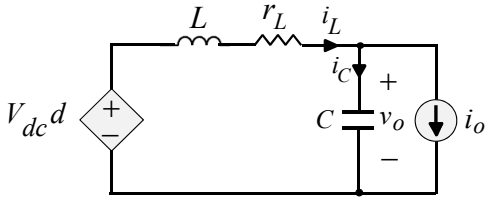

Fig. 6. Single-phase representation of the DG inverter.

As shown in Fig. 3, only positive sequence current is passing through virtual impedance. In this way, increase of DG output voltage unbalance due to the negative sequence voltage drop on the virtual impedance will be avoided.

D. Voltage and Current Controllers

Due to the difficulties of using PI controllers to track non-dc variables, proportional-resonant (PR) controllers are usually preferred to control the voltage and current in the stationary reference frame [47]. In this paper, PR voltage and current controllers are as (14) and (15):

$$G_V(s) = k_{pV} + \frac{2k_{rV}\cdot\omega_{cV}\cdot s}{s^2 + 2\omega_{cV}\cdot s + \omega_0^2} \tag{14}$$

$$G_I(s) = k_{pI} + \frac{2k_{rI}\cdot\omega_{cI}\cdot s}{s^2 + 2\omega_{cI}\cdot s + \omega_0^2} \tag{15}$$

where, k_{pV} (k_{pI}) and k_{rV} (k_{rI}) are the proportional and resonant coefficients of the voltage (current) controller, respectively. Also, ω_{cV} and ω_{cI} represent the voltage and current controller cut-off frequencies, respectively.

IV. Control System Design and Stability Analysis

A. Primary Control Level

The design and stability analysis of the droop controllers are sufficiently studied in the literature (e.g. [28]-[31]) and will not be discussed. Thus, in this Subsection, voltage, current and virtual impedance control loops are designed; then, in the next Subsection, stability of unbalance compensation is evaluated.

According to the symmetrical components theory [48], an unbalanced electrical system can be analyzed by separate positive and negative sequence balanced systems. Thus, the single-phase representation of the DG inverter which is shown in Fig. 6 is considered for modeling of positive (or negative) sequence control system.

Based on Fig. 6, the output voltage dynamics [31] can be derived:

$$v_o = \frac{V_{dc}}{LCs^2 + r_L Cs + 1}d - \frac{Ls + r_L}{LCs^2 + r_L Cs + 1}i_o \tag{16}$$

where d and r_L are the duty cycle and filter inductor resistance, respectively.

On the other hand, according to Fig. 3, the block diagram of local control system and power stage for positive (or negative) sequence is achieved as Fig. 7. Based on this Fig., the following equation can be extracted:

$$V_{dc}d = \left[(v^* - v_o - Z_v\cdot i_o)G_V(s) - i_L\right]G_I(s) \tag{17}$$

where $Z_v = r_v + L_v s$.

Finally, replacing $V_{dc}d$ from (17) in (16), and taking into account that $i_L = C\frac{dv_o}{dt} + i_o$ result in the following equation:

$$v_o = G(s)\cdot v^* - Z_o(s)\cdot i_o \tag{18}$$

where $G(s)$ and $Z_o(s)$ are the control system closed-loop transfer function and output impedance, respectively and represent the equivalent Thevenin circuit of the closed loop system:

$$G(s) = \frac{A}{LCs^2 + r_L Cs + 1 + B}$$

$$Z_o(s) = \frac{A\cdot Z_v + r_L + Ls}{LCs^2 + r_L Cs + 1 + B}$$

being:

$$A = \frac{G_I(s).G_V(s)}{1 + \frac{G_I(s)}{r_L + Ls}}$$

$$B = \frac{G_I(s) - (r_L + Ls)G_I(s).G_V(s)}{(r_L + Ls) + G_I(s)}$$

It is noteworthy that in these equations and also Fig. 7, virtual impedance loop is only considered for positive sequence. Furthermore, as seen in Fig. 7, it is necessary to replace s by $-s$ for negative sequence.

The positive and negative sequence Bode diagrams of $G(s)$ and $Z_o(s)$ by considering the power stage and primary control system parameters (listed in Tables I and II) are depicted in Figs. 8 and 9, respectively.

As can be seen in Fig. 8, the magnitude of $G(s)$ is the same for positive and negative sequences. Also, as expected, positive and negative sequences are in the opposite phase. Furthermore, the gain and the phase angle of closed-loop transfer function at fundamental frequency are respectively unity and zero for both positive and negative sequences. Thus, proper tracking of voltage reference is ensured.

As shown in Fig. 9, magnitude of negative sequence output impedance at fundamental frequency is very low, because, as mentioned before, the virtual impedance is only acting for positive sequence.

B. Stability Analysis of Unbalance Compensation

Since, the main contribution of this paper is the PCC voltage unbalance compensation; the compensated system stability is evaluated in this Subsection.

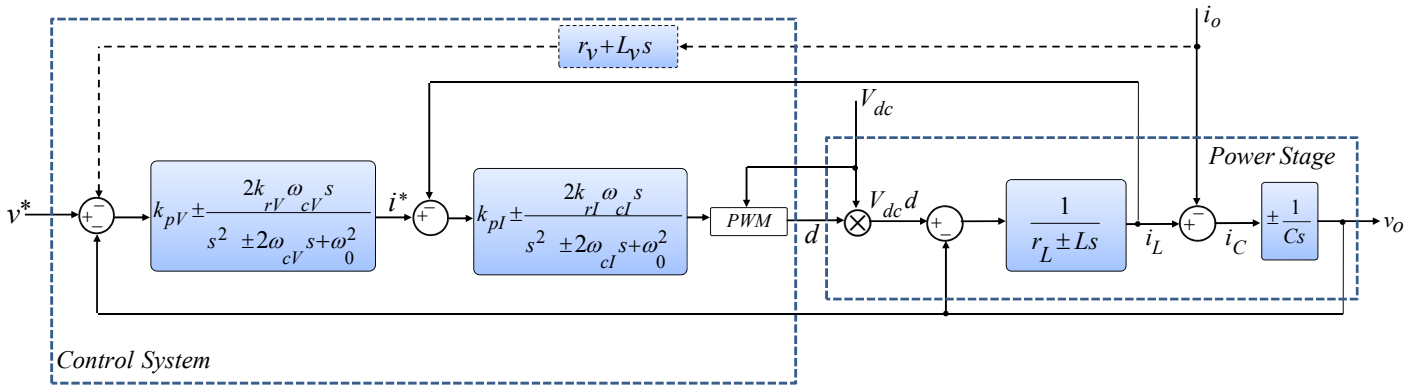

Fig. 7. Block diagram of power stage and control system for positive/negative sequence.

According to Figs. 1-3, *UCR* is generated in *dq* frame, but, finally is transformed to and acting in *αβ* frame. Thus, here, unbalance compensation is modeled in *αβ* frame. Unbalance compensation block diagram depicted in Fig. 2 is equivalent to the following stationary frame equation:

$$UCR_\alpha = (VUF^* - VUF)\cdot PI\cdot v_\alpha^- \tag{19}$$

where *PI* represents the controller $(k_P + \frac{k_I}{s})$.

According to Fig. 4, *VUF* at PCC can be calculated as equation (20):

$$VUF = \frac{\bar{v}_\alpha^-}{\bar{v}_\alpha^+}\cdot 100 = \frac{abs(v_\alpha^-)\cdot LPF}{abs(v_\alpha^+)\cdot LPF}\cdot 100 = \frac{abs(v_\alpha^-)\cdot LPF}{230\sqrt{3}\cdot\frac{2}{\pi}}\cdot 100 \tag{20}$$

As mentioned before, $\bar{v}_\alpha^-$ and $\bar{v}_\alpha^+$ are the average values of PCC negative and positive sequence rectified voltages, respectively. *LPF* transfer function is same as equation (1).

In order to calculate the denominator of (20), the positive sequence voltage drops caused by reactive power droop controller and distribution line impedances are neglected. Thus, the amplitude of PCC positive sequence phase voltage can be approximated by $230\sqrt{2}$, assuming 230 V as the rated rms value of phase voltage. This amplitude is equal to $230\sqrt{3}$ in *αβ* frame according to Clarke transformation equations which can be found in [22]. Also, it should be noted that the output of *abs* function is a full-wave rectified sinusoidal waveform. Thus, its average can be calculated through multiplying the phase voltage peak value by $\frac{2}{\pi}$ (i.e. $\bar{v}_\alpha^+ = 230\sqrt{3}\cdot\frac{2}{\pi}$).

It is noteworthy that (19) and (20) are also valid for *β*-component.

As can be seen in Fig. 1, 2nd order *LPF*s with the transfer function of (1) are used for v_{dq}^- and v_{dq}^+ extraction. Thus, the dynamics of equation (19) is same as the original unbalance compensation control system which is in *dq* frame.

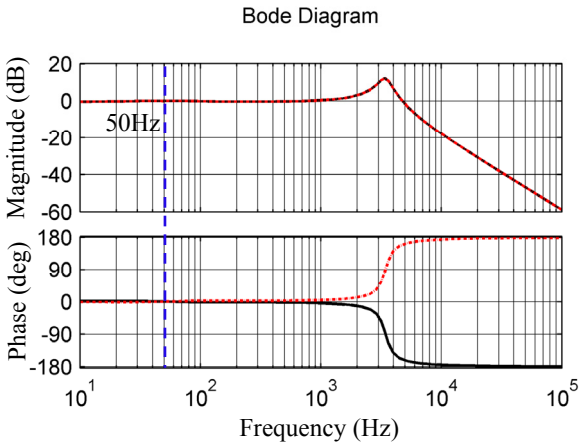

Fig. 8. Bode diagrams of positive (solid line) and negative (dashed line) sequence closed-loop transfer function.

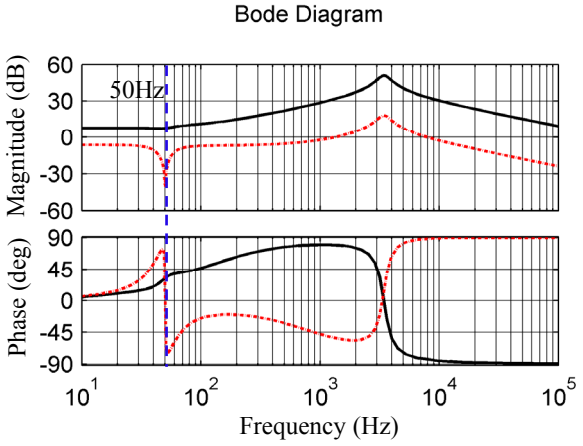

Fig. 9. Bode diagrams of positive (solid line) and negative (dashed line) sequence output impedance.

By replacing (20) in (19) and assuming *VUF**=0.5% and $abs(v_\alpha^-) = \pm v_\alpha^-$, the following equation is achieved:

$$UCR_\alpha = \left[0.5v_\alpha^- \pm 0.39(v_\alpha^-)^2.LPF\right]\cdot PI \tag{21}$$

Since, (21) is a nonlinear equation, its small-signal representation is extracted as follows:

$$\hat{UCR}_\alpha = \left[0.5\hat{v}_\alpha^- \pm 0.78v_\alpha^-\cdot\hat{v}_\alpha^-.LPF\right]\cdot PI \tag{22}$$

where the symbol ^ represents the small signal value.

On the other hand, according to the symmetrical components theory [48], when a single-phase load is connected between two phases (the case considered in this paper), the circuit shown in Fig. 10(a) which is constructed by the connection of positive and negative sequence equivalent circuits can be used for the negative sequence current calculation. In this Fig., Z_{UB}, Z^+ and Z^- are unbalanced load impedance and positive and negative sequence equivalent impedances, respectively. v^+_{source}, v^+ and v^- represent the ac source positive sequence output voltage and PCC positive and negative sequence voltages, respectively.

This circuit is depicted for a microgrid consisting of two DGs as Fig. 10(b), where $Z_{\ell k}$ and Z^-_{ok} (k=1,2) are the distribution line impedance (the line between DG_k and PCC) and DG_k negative sequence output impedance, respectively and $i^-_{o_{\alpha k}}$ is DG_k negative sequence α-component output current.

The values of Z_{UB}, $Z_{\ell 1}$ and $Z_{\ell 2}$ can be found in Table I. Thus, according to Fig. 10(b) and considering this fact that $Z_{UB} >> Z_{\ell 1}, Z_{\ell 2}$ and $Z^-_{o1} = Z^-_{o2} = Z^-_o$, the following equations are achieved:

$$i^-_\alpha \approx \frac{v^+_\alpha}{Z_{UB}} \tag{23}$$

$$v^-_\alpha \approx F \cdot v^+_\alpha \tag{24}$$

being,

$$F = -\frac{(Z_{\ell 1} + Z^-_o)\cdot(Z_{\ell 2} + Z^-_o)}{(Z_{\ell 1} + Z^-_o) + (Z_{\ell 2} + Z^-_o)} \cdot \frac{1}{Z_{UB}} \tag{24a}$$

In equation (24a), $Z_{\ell 1}$ and $Z_{\ell 2}$ should be replaced according to Table I as 0.6-0.0054s (Ω) and 0.2-0.0018s (Ω), respectively. It is noteworthy that "-s" should be used instead of "s" in negative sequence Laplace-domain equations.

Bode diagrams of $Z_{\ell 1}$, $Z_{\ell 2}$ and Z^-_o are compared in Fig. 11. According to this Fig., Z^-_o is negligible in comparison with $Z_{\ell 1}$ and $Z_{\ell 2}$, except in the low-frequency range. Thus, F can be approximated as:

$$F \approx -\frac{Z_{\ell 1}\cdot Z_{\ell 2}}{Z_{\ell 1} + Z_{\ell 2}} \cdot \frac{1}{Z_{UB}} \tag{25}$$

Then, replacing (24) in (22) leads to the following equation:

$$U\hat{C}R_\alpha = \left[\hat{v}^-_\alpha (0.5 \pm 0.78F \cdot v^+_\alpha . LPF)\right] \cdot PI \tag{26}$$

In this equation, v^+_α should be replaced by its Laplace-domain form:

$$v^+_\alpha \approx L\left(230\sqrt{3}\cdot\sin(\omega_0 t)\right) = \frac{230\sqrt{3}\,\omega_0}{s^2 + \omega_0^2} \tag{27}$$

where $L(\bullet)$ represent the Laplace transform.

On the other hand, (18) can be written in the following negative sequence small-signal form:

$$\hat{v}^-_{o_\alpha} = G^-(s)\cdot U\hat{C}R_\alpha - Z^-_o(s)\cdot i^-_{o_{\alpha k}} \tag{28}$$

Note that according to Fig. 3, $\hat{v}^*_\alpha = U\hat{C}R_\alpha$. Moreover, $i^-_{o_{\alpha k}}$ can be easily calculated according to Fig. 10(b); however, due to low value of the negative sequence output impedance (especially at fundamental frequency), $Z^-_o(s)\cdot i^-_{o_{\alpha k}}$ is neglected to extract the following closed loop transfer function:

$$H = \frac{\hat{v}^-_{o_\alpha}}{\hat{v}^-_\alpha} = G^-(s)\cdot(0.5 \pm 0.78F \cdot v^+_\alpha . LPF)\cdot PI \tag{29}$$

Considering the parameters of Tables I and II, poles of H are depicted in Fig. 12. As seen, all the poles are in the left-half of s-plane; thus, the stability of the control system is guaranteed.

It should be noted that according to (29), the parameters of the PI controller (k_P and k_I) has no effect on the control system stability.

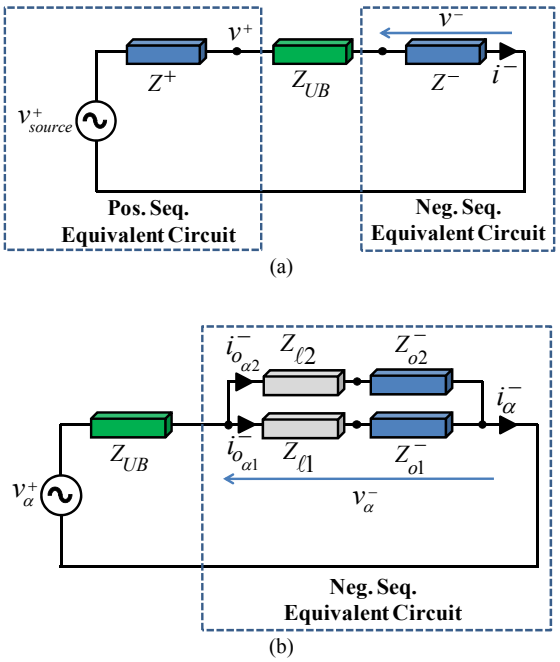

Fig. 10. Equivalent circuit for calculation of negative sequence current.
(a) Basic circuit according to symmetrical component theory
(b) Equivalent circuit for α-component in a two-DG microgrid

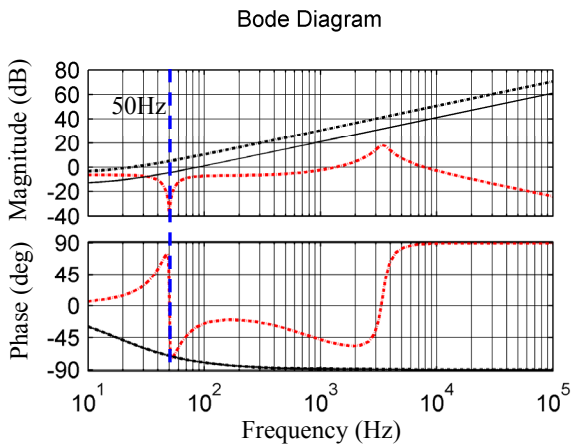

Fig. 11. Bode diagrams of Z_o^- (red dashed line), $Z_{\ell 1}$ (black dashed line) and $Z_{\ell 2}$ (solid line).

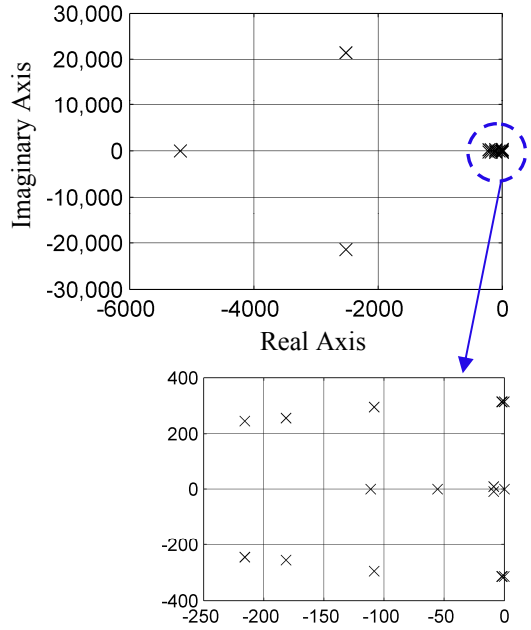

Fig. 12. Poles of compensated system transfer function (H).

V. Simulation Results

The islanded microgrid of Fig. 13 is considered as the test system. This microgrid includes two DGs with power stage and control system shown in Figs. 1-3. Power stage and control system parameters are listed in Tables I and II, respectively. Switching frequency of the DGs inverters is set to 10 kHz. As seen in Fig. 13, a single-phase load (Z_{UB}) is connected between phases "a" and "b" which creates voltage unbalance. A balanced star-connected three-phase load (Z_B) is also connected to PCC. In this Fig., $Z_{\ell 1}$ and $Z_{\ell 2}$ represent the distribution lines between DGs and PCC.

Unbalance compensation starts acting from t=2.5sec. VUF^* is set to 0.5%.

As shown in Fig. 14, VUF of PCC follows the reference value, properly. Also, it can be seen that the improvement of PCC voltage quality is achieved by making the DGs output voltage unbalanced. Also, because of the less line impedance between DG_2 and the PCC; its VUF is increased a little more.

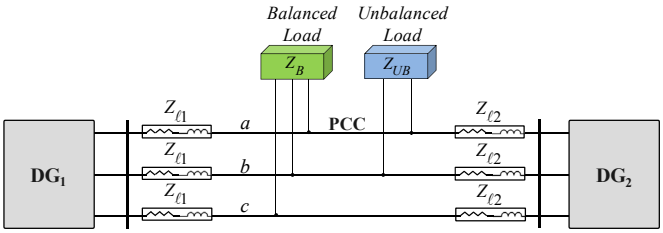

Fig. 13. Test system of simulation studies.

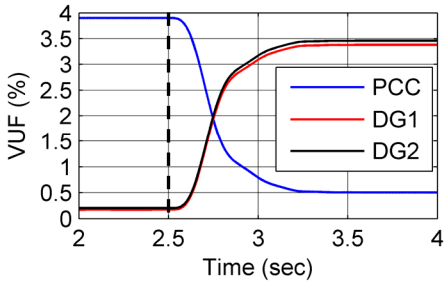

Fig. 14. VUF at PCC and DGs terminal.

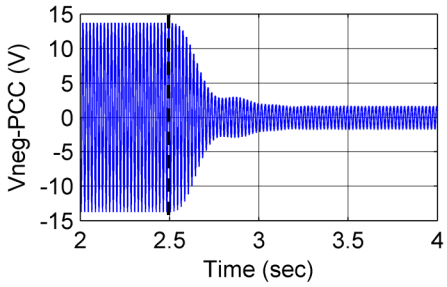

(a)

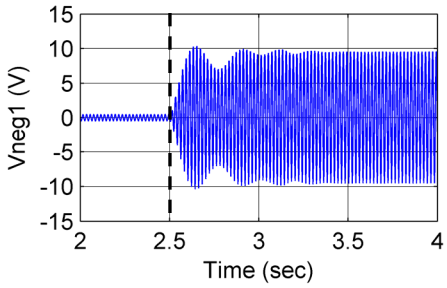

(b)

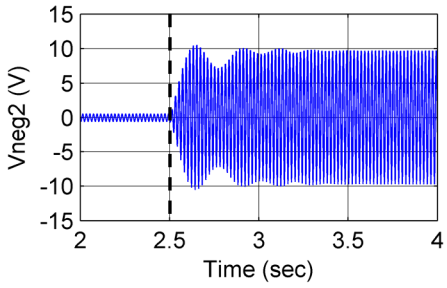

(c)

Fig. 15. Phase-a negative sequence voltage of : (a) PCC, (b) DG_1, (c) DG_2.

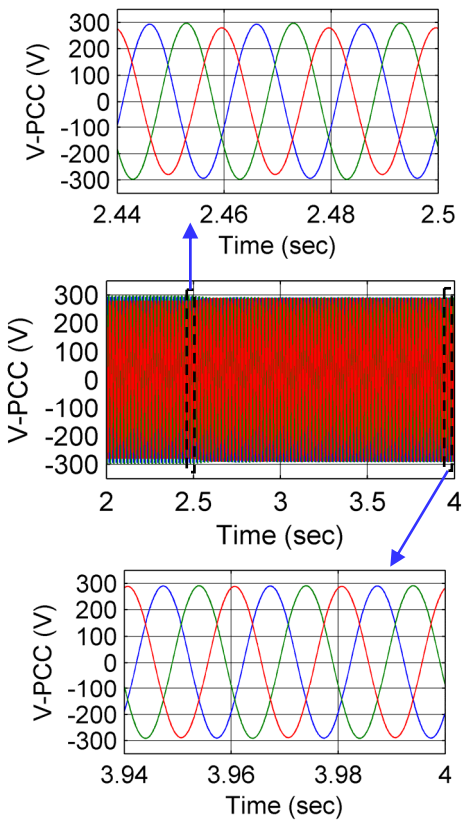

Fig. 16. Three-phase voltages: (a) PCC, (b) DG_1 terminal.

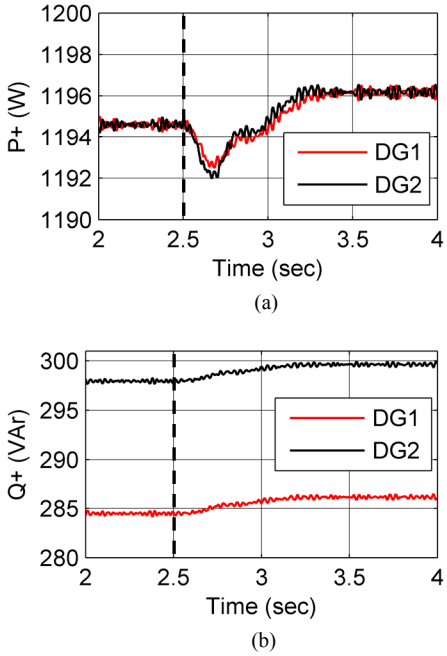

Fig. 17. Power sharing: (a) active power, (b) reactive power.

To provide more details, phase-*a* negative sequence voltages at PCC and DGs terminal are shown in Figs. 15(a)-(c). As seen, PCC negative sequence voltage is decreased by increase of DGs output voltage negative sequence.

Also, in order to demonstrate unbalance compensation more clearly, three-phase output voltages at PCC and DG_1 terminal are shown in Figs. 16(a) and 16(b), respectively. DG_2 output voltage behavior is similar to DG_1. As seen, as a result of compensation, PCC voltage unbalance is decreased, effectively; while, the DG output voltage becomes unbalanced.

Sharing of P^+ and Q^+ between DGs are shown in Figs. 17(a) and 17(b), respectively. As seen, in spite of asymmetrical distribution lines ($Z_{\ell 1} = 3Z_{\ell 2}$), active and reactive powers are shared properly between the DGs. It can be seen that the effect of unbalance compensation on positive sequence powers is quite negligible; since, compensation is acting over negative sequence.

Also, it should be noted that the active power can be shared exactly between DGs, because, the frequency is the same throughout the microgrid, while, due to non-uniform profile of microgrid voltage, reactive power is shared by a small error.

VI. Conclusions

A hierarchical control approach for PCC voltage unbalance compensation in an islanded microgrid is proposed. The control structure consists of DGs local controllers (primary level), and a central secondary controller. The secondary controller manages PCC voltage unbalance compensation by sending proper control signals to the primary level. PCC voltage data and the control signal are transmitted to/from secondary level through low bandwidth communication links.

TABLE I
POWER STAGE PARAMETERS

DG prime mover	inverter filter inductance	inverter filter capacitance	DG_1 distribution line	DG_2 distribution line	Unbalanced load	Balanced load
$V_{dc}\,(V)$	$L(mH)$	$C\,(\mu F)$	$Z_{\ell 1}(\Omega)$	$Z\ell 2\ (\Omega)$	$Z_{UB}(\Omega)$	$Z_B(\Omega)$
650	1.8	25	0.6+j1.6965	0.2+j0.5655	600	50+j12.57

TABLE II
CONTROL SYSTEM PARAMETERS

Primary Level													Secondary Level	
Power Controllers					Virtual Impedance		Voltage Controller			Current Controller			PI Controller	
m_D	m_P	n_P	E_0	ω_0	R_v (Ω)	L_v (mH)	k_{pV}	k_{rV}	ω_{cV}	k_{pI}	k_{rI}	ω_{cI}	k_P	k_I
0.00002	0.0002	0.13	$230\sqrt{2}$	2π*50	1	4	2	100	2	10	1000	2	0.5	7

The control system design and stability analysis are discussed. The presented simulation results show that the PCC voltage unbalance is compensated to the desired value, while active and reactive powers are shared properly.

As the next step, we are working on the secondary control for compensation of the other PCC voltage power quality problems such as voltage harmonics and sags.

REFERENCES

[1] E. Santacana, G. Rackliffe, L. Tang, and X. Feng, "Getting smart," *IEEE Power and Energy Mag.*, vol. 8, no. 2, pp. 41-48, Mar./Apr. 2010.

[2] S. Bruno, S. Lamonaca, G. Rotondo, U. Stecchi, and M. La Scala, "Unbalanced three-phase optimal power flow for smart grids," *IEEE Trans. Ind. Electron.*, vol. 58, no. 10, pp. 4504-4513, Oct. 2011.

[3] H. Farhangi, "The path of the smart grid," *IEEE Pow. and Energy Mag.*, vol. 8, no. 1, pp. 18-28, Jan./Feb. 2010.

[4] P. P. Varaiya, F. F. Wu, and J. W. Bialek, "Smart operation of smart grid: risk-limiting dispatch," *Proc. of the IEEE*, vol. 99, no. 1, pp. 40-57, Jan. 2011.

[5] R. H. Lasseter, "Smart distribution: coupled microgrids," *Proc. of the IEEE*, vol. 99, no. 6, pp. 1074-1082, Jun. 2011.

[6] X. Liu, P. Wang, and P. C. Loh, "A hybrid ac/dc microgrid and its coordination control," *IEEE Trans. Smart Grid*, vol. 2, no. 2, pp. 278-286, Jun. 2011.

[7] A. A. Aquino-Lugo, R. Klump, and T. J. Overbye, "A control framework for the smart grid for voltage support using agent-based technologies," *IEEE Trans. Smart Grid*, vol. 2, no. 1, pp. 173-180, Mar. 2011.

[8] K. Moslehi, and R. Kumar, "A reliability perspective of the smart grid," *IEEE Trans. Smart Grid*, vol. 1, no. 1, pp. 57-64, Jun. 2010.

[9] *IEEE Guide for Design, Operation, and Integration of Distributed Resource Island Systems with Electric Power Systems*, IEEE Standard 1547.4-2011, 2011.

[10] F. Katiraei, R. Iravani, N. Hatziargyriou, and A. Dimeas, "Microgrids management," *IEEE Power and Energy Mag.*, vol. 6, no. 3, pp. 54-65, May/Jun. 2008.

[11] A. G. Tsikalakis, and and N. D. Hatziargyriou, "Centralized control for optimizing microgrids operation," *IEEE Trans. Energy Conv.*, vol. 23, no. 1, pp. 241-248, Mar. 2008.

[12] A. V. Jouanne, and B. Banerjee, "Assessment of voltage unbalance," *IEEE Trans. Power Deliv.*, vol. 16, no. 4, pp. 782–790, Oct. 2001.

[13] F. Barrero, S. Martínez, F. Yeves, F. Mur, and P. Martínez, "Universal and reconfigurable to UPS active power filter for line conditioning," *IEEE Trans. Power Deliv.*, vol. 18, no. 1, pp. 283-290, Jan. 2003.

[14] D. Graovac, V. A. Katic´, and A. Rufer, "Power quality problems compensation with universal power quality conditioning system," *IEEE Trans. Power Deliv.*, vol. 22, no. 2, pp. 968-976, Apr. 2007.

[15] B. Singh, K. Al-Haddad, and A. Chandra, "A review of active filters for power quality improvement," *IEEE Trans. Ind. Electron.*, vol. 46, no. 5, pp. 960-971, Oct. 1999.

[16] A. G. Cerrada , O. P. Ardila, V. F. Batlle, P. R. Sánchez, and P. G. González, "Application of a repetitive controller for a three-phase active power filter," *IEEE Trans. Power Electron.*, vol. 22, no. 1, pp. 237-246, Jan. 2007.

[17] A. Chandra, B. Singh, B. N. Singh, and K. Al-Haddad, "An improved control algorithm of shunt active filter for voltage regulation, harmonic elimination, power factor correction, and balancing of nonlinear loads," *IEEE Trans. Power Electron.*, vol. 15, no. 3, pp. 495-507, May 2000.

[18] B. Singh, and J. Solanki, "An implementation of an adaptive control algorithm for a three-phase shunt active filter," *IEEE Trans. Ind. Electron.*, vol. 56, no. 8, pp. 2811-2820, Aug. 2009.

[19] S. George, and V. Agarwal, "A DSP based optimal algorithm for shunt active filter under nonsinusoidal supply and unbalanced load conditions," *IEEE Trans. Power Electron.*, vol. 22, no. 2, pp. 593-601, Mar. 2007.

[20] M. Hojo, Y. Iwase, T. Funabashi, and Y. Ueda, "A method of three-phase balancing in microgrid by photovoltaic generation systems," in *Proc. 2008, Pow. Elec. and Motion Cont. Conf. (EPE-PEMC)*, pp. 2487-2491.

[21] P. T. Cheng, C. Chen, T. L. Lee and S. Y. Kuo, "A cooperative imbalance compensation method for distributed-generation interface converters," *IEEE Trans. Ind. Appl.*, vol. 45, no. 2, pp. 805-815, Mar./Apr. 2009.

[22] M. Savaghebi, J. M. Guerrero, A. Jalilian, and J. C. Vasquez, "Experimental evaluation of voltage unbalance compensation in an islanded microgrid," in *Proc. 2011, 20th IEEE Int. Symp. Ind. Electron. (ISIE 2011)*, pp. 1453-1458.

[23] M. Savaghebi, A. Jalilian, J. C. Vasquez, J. M. Guerrero, and R. Teodorescu, "Distributed generator with voltage unbalance compensation capability," in *Proc. 2010, 25th Int. Power Sys. Conf. (PSC 2010)*, pp. 1-10. (available online: www.psc-ir.com/ed10/10-E-PQA-1943.pdf) .

[24] J. M. Guerrero, J. C. Vasquez, J. Matas, L. G. de Vicuña, and M. Castilla, "Hierarchical control of droop-controlled AC and DC microgrids—a general approach toward standardization," *IEEE Trans. Ind. Electron.*, vol. 58, no. 1, pp. 158-172, Jan. 2011.

[25] A. Madureira, C. Moreira, and J. P. Lopes, "Secondary load-frequency control for microgrids in islanded operation," in *Proc. 2005, Int. Conf. Renewable energies and Pow. Quality (ICREPQ)*, pp. 1-4.

[26] J. P. Lopes, C. Moreira, and A. G. Madureira, "Defining control strategies for microgrids islanded operation," *IEEE Trans. Power Sys.*, vol. 21, no. 2, pp. 916-924, May 2006.

[27] A. Mehrizi-Sani and R. Iravani, "Potential-function based control of a microgrid in islanded and grid-connected modes," *IEEE Trans. Power Sys.*, vol. 25, no. 4, pp. 1883-1891, Nov. 2010.

[28] J. M. Guerrero, J. Matas and L. G. de Vicuña, M. Castilla, and J. Miret, "Decentralized control for parallel operation of distributed generation inverters using resistive output impedance," *IEEE Trans. Ind. Electron.*, vol. 54, no. 2, pp. 994-1004, Apr. 2007.

[29] E. Barklund, N. Pogaku, M. Prodanovic´, C. H. Aramburo, and T. C. Green, "Energy management in autonomous microgrid using stability-constrained droop control of inverters," *IEEE Trans. Power Electron.*, vol. 23, no. 5, pp. 2346-2352, Sept. 2008.

[30] Y. Li, D. M. Vilathgamuwa, and P. C. Loh, "Design, analysis, and real-time testing of a controller for multibus microgrid system," *IEEE Trans. Power Electron.*, vol. 19, no. 5, pp. 1195-1204, Sept. 2004.

[31] J. M. Guerrero, L. G. Vicuna, J. Matas, M. Castilla, and J. Miret, "Output impedance design of parallel-connected UPS inverters with wireless load sharing control," *IEEE Trans. Ind. Electron.*, vol. 52, no. 4, pp. 1126-1135, Aug. 2005.

[32] J. He, and Y. W. Li "Analysis and design of interfacing inverter output virtual impedance in a low voltage microgrid," in *Proc. 2010, Energy Conv. Cong. and Exp. (ECCE)*, pp. 2857–2864.
[33] F. Katiraei, and M.R. Iravani, "Power management strategies for a microgrid with multiple distributed generation units", *IEEE Trans. Power Sys.*, vol. 21, no.4, pp. 1821-1831, Nov. 2006.
[34] A. Pantoja, and N. Quijano, "A population dynamics approach for the dispatch of distributed generators," *IEEE Trans. Ind. Electron*, vol 58, no. 10, pp. 4559-4567, Oct. 2011.
[35] M. Meiqin, D. Wei, and L. Chang, "Multi-agent based simulation for microgrid energy management," in *Proc. 2011, IEEE 8th Int. Conf. Power Electron. and ECCE Asia (ICPE & ECCE)*, pp. 1219–1223.
[36] S. Suryanarayanan, J. Mitra, and S. Biswas, "A conceptual framework of a hierarchically networked agent-based microgrid architecture," in *Proc. 2010, IEEE PES Trans. and Dist. Conf. and Exp.*, pp. 1–5.
[37] B. Kroposki, R. Lasseter, T. Ise, S. Morozumi, S. Papatlianassiou, and N. Hatziargyriou, "Making microgrid work," *IEEE Power and Energy Mag.*, vol. 6, no. 3, pp. 40-53, May/Jun. 2008.
[38] I. Serban, and C. Marinescu, "Frequency control issues in microgrids with renewable energy sources," in *Proc. 2011, 7th Int. Symp. Advanced Topics in Elec. Eng. (ATEE)*, pp. 1-6.
[39] K. Vanthournout, K. De Brabandere, E. Haesen, J. Van den Keybus, G. Deconinck, and R. Belmans, "Agora: distributed tertiary control of distributed resources," in *Proc.* 2005, *15th Power Sys. Comput. Conf.*, pp. 1-7.
[40] A. G. Madureira and J. P. Lopes, "Voltage and reactive power control in MV networks integrating microgrids," in *Proc. 2007, Int. Conf. Renewable energies and Pow. Quality (ICREPQ)*, pp. 1-5.
[41] P. Jintakosonwit, H. Akagi, H. Fujita, and S. Ogasawara, "Implementation and performance of automatic gain adjustment in a shunt active filter for harmonic damping throughout a power distribution system," *IEEE Trans. Power Electron.*, vol. 17, no. 3, pp. 438-447, Mar. 2002.
[42] Y. Li, D. M. Vilathgamuwa, and P. C. Loh, "A grid-interfacing power quality compensator for three-phase three-wire microgrid applications," *IEEE Trans. Power Electron.*, vol. 21, no. 4, pp. 1021-1031, Jul. 2006.
[43] M. Ciobotaru, R. Teodorescu, and F. Blaabjerg, "A new single-phase PLL structure based on second order generalized integrator," *in Proc. 2006, Power Electron. Specialists Conf. (PESC)*, pp. 1-6.
[44] P. Rodriguez, A. V. Timbus, R. Teodorescu, M. Liserre and F. Blaabjerg, "Flexbile active power control of distributed power generation systems during grid faults," *IEEE Trans. Ind. Electron.*, vol. 54, no. 5, pp. 2583-2592, Oct. 2007.
[45] H. Akagi, Y. Kanagawa, and A. Nabase, "Instantaneous reactive power compensator comprising switching devices without energy storage components," *IEEE Trans. Ind. Appl.*, vol. IA-20, no. 3, p. 625, May/Jun. 1984.
[46] F. Z. Peng, G. W. Ott, and D. J. Adams, "Harmonic and reactive power compensation based on the generalized instantaneous reactive power theory for three-phase four-wire systems," *IEEE Trans. Power Electron.*, vol. 13, no. 6, pp. 1174-1181, Nov. 1998.
[47] F. Blaabjerg, R. Teodorescu, M. Liserre and A. V. Timbus, "Overview of control and grid synchronization for distributed power generation systems," *IEEE Trans. Ind. Elec.*, vol. 53, no. 5, pp. 1398-1409, Oct. 2006.
[48] J. D. Glover, and M. Sarma, *Power System Analysis and Design- 2nd Edition*, Boston: PWS Publishing Company, 1993.

Mehdi Savaghebi (S'06) was born in Karaj, Iran, in 1983. He received the B.S. degree from Tehran University, Iran, in 2004 and the M.S. degree with highest honors from Iran University of Science and Technology (IUST), in 2006, both in electrical engineering. He is now perusing the Ph.D. degree in IUST.

His main research interests include Distributed Generation systems, Microgrids and power quality issues of electrical systems.

Alireza Jalilian was born in Yazd, Iran, in 1961. He received the B.S. degree in electrical engineering from Mazandaran University, Babol, Iran, in 1989, and the M.S. and Ph.D. degrees from the University of Wollongong, Wollongong, New South Wales, Australia, in 1992 and 1997, respectively.

He joined the Power Group of the Department of Electrical Engineering at the Iran University of Science and Technology in 1998, where he is an Assistant Professor. His research interests are power-quality problems causes and effects as well as mitigation methods.

Juan C. Vasquez received the B.S. degree in Electronics Engineering from Autonoma University of Manizales, Colombia, in 2004 where he has been teaching courses on digital circuits, servo systems and flexible manufacturing systems. In 2009, he has received his Ph.D. degree from the Technical University of Catalonia, Barcelona, Spain in 2009 at the Department of Automatic Control Systems and Computer Engineering, from Technical University of Catalonia, Barcelona Spain, where he worked as a Post-doc Assistant and also taught courses based on renewable energy systems. Currently, he is an Assistant Professor in Aalborg University, Denmark. His research interests include modeling, simulation, and power management applied to the Distributed Generation in Microgrids.

Josep M. Guerrero (S'01–M'03–SM'08) was born in Barcelona, Spain, in 1973. He received the B.S. degree in telecommunications engineering, the M.S. degree in electronics engineering, and the Ph.D. degree in power electronics from the Technical University of Catalonia, Barcelona, Spain, in 1997, 2000 and 2003, respectively.

He is an Associate Professor with the Department of Automatic Control Systems and Computer Engineering, Technical University of Catalonia, Barcelona, where he currently teaches courses on digital signal processing, FPGAs, microprocessors, and renewable energy. Since 2004, he has been responsible for the Renewable Energy Laboratory, Escola Industrial de Barcelona. He has been a visiting Professor at Zhejiang University, China, and University of Cergy-Pontoise, France. From 2011, he is a Full Professor at the Department of Energy Technology, Aalborg University, Denmark, where he is the responsible of the Microgrids research program. His research interests is oriented to different Microgrids aspects, including power electronics, distributed energy storage systems, hierarchical and cooperative control, energy management systems and optimization of microgrids and islanded minigrids.

Dr. Guerrero is an Associate Editor for the IEEE TRANSACTIONS ON POWER ELECTRONICS, IEEE TRANSACTIONS ON INDUSTRIAL ELECTRONICS, and IEEE INDUSTRIAL ELECTRONICS MAGAZINE. He has been Guest Editor of the IEEE Transactions on Power Electronics Special Issues: Power Electrics for Wind Energy Conversion and Power Electronics for Microgrids; and the IEEE Transactions on Industrial Electronics Special Sections: Uninterruptible Power Supplies (UPS) systems, Renewable Energy Systems, Distributed Generation and Microgrids, and Industrial Applications and Implementation Issues of the Kalman Filter He currently chairs the Renewable Energy Systems Technical Committee of IEEE IES.